Experimental and Theoretical Charge Density Distribution in Pigment Yellow 101

Jonathan J. Du[a], Yiliang Zhao[a], Linda Váradi[a], James A. Platts[b], Paul W. Groundwater[a], and David E. Hibbs[*a]

[a] Faculty of Pharmacy, The University of Sydney, NSW 2006, Australia.

[b] School of Chemistry, Cardiff University, Park Place, Cardiff, CF10 3AT, UK.

Abstract

The charge density distribution in 2,2'-Dihydroxy-1,1'-naphthalazine (Pigment Yellow 101; P.Y.101) has been determined using high-resolution X-ray diffraction and multipole refinement, along with density functional theory calculations. Topological analysis of the resulting densities highlights the localisation of single/double bonds in the central C=N-N=C moiety of the molecule in its ground state. The density in the N—N is examined in detail, where we show that very small differences between experiment and theory are amplified by use of the Laplacian of the density. Quantification of hydrogen bonds highlights the importance of the intramolecular N—H…O interaction, known to be vital for retention of fluorescence in the solid state, relative to the many but weak intermolecular contacts located. However, a popular method for deriving H-bond strengths from density data appears to struggle with the intramolecular N—H…O interaction. We also show that theoretical estimation of anisotropic displacements for hydrogen atoms brings little benefit overall, and degrades agreement with experiment for one intra-molecular contact.

Introduction

2,2'-Dihydroxy-1,1'-naphthalazine (Pigment Yellow 101; P.Y.101) **1** has been produced industrially since its discovery in 1899.[1] It is a bis-azomethine type colourfast pigment used as a result of its strong yellow colour, photostability, and low solubility in organic solvents. Despite its long history of use, until recently little attention had been paid to the solid state fluorescence of P.Y.101. P.Y.101 is the only example of an organic or inorganic pigment used commercially which exhibits sold state fluorescence.[2] The synthesis of P.Y.101 is straightforward, involving the condensation of 2 equivalents of 2-hydroxy-1-naphthaldehyde with the 1 equivalent of hydrazine hydrate in ethanol, and heating on a water bath for 1 hour.[3] On cooling the fluorescent solution, P.Y.101 is obtained as a yellow fluorescent solid which, if required, can be further purified by recrystallization from DMF.[2]

Fluorescent organic pigments do not usually contain phenolic groups since they provide a non-radiative decay pathway *via* hydrogen transfer. For P.Y.101, however, quantum chemical studies using time-dependent density functional theory (TDDFT) have shown that intramolecular hydrogen bonding of this OH (donor) to the azomethine N (acceptor) leads to sufficient stabilization of the lone-pair orbital and an increase in the excitation energy for the forbidden n-π* state which would otherwise promote fluorescence quenching.[2] The S_1 state for P.Y.101 is the result of a π-π* transition, and it is from this state that fluorescence takes place.[4] For P.Y.101, the intramolecular hydrogen bonds are thus essential for fluorescence and absence of OH groups leads to loss of fluorescence.

Steady state spectroscopy and density functional theory (DFT) and TDDFT have shown that, in solution, the *trans*-diol tautomer **1** is the most stable ground state conformer, and excitation takes place to the *trans*-diol excited state **1***, Scheme 1. The trans-diol excited state **1*** can tautomerize to the *trans*-keto form **2*** by excited-state intramolecular proton transfer (ESIPT), and this *trans*-keto form **2*** can decay to the *trans*-diol **1*** excited state *via* retro-ESIPT and also, *via* fluorescence, to the ground state *trans*-keto form **2**. A minor fraction of the excited state undergoes *trans-cis* isomerization, to give the *cis*-diol (not shown) and *cis*-keto **3*** forms.[5] In the solid state, this *trans-cis* isomerization is not observed in the excited state. Other non-radiative decay pathways exist.[6]
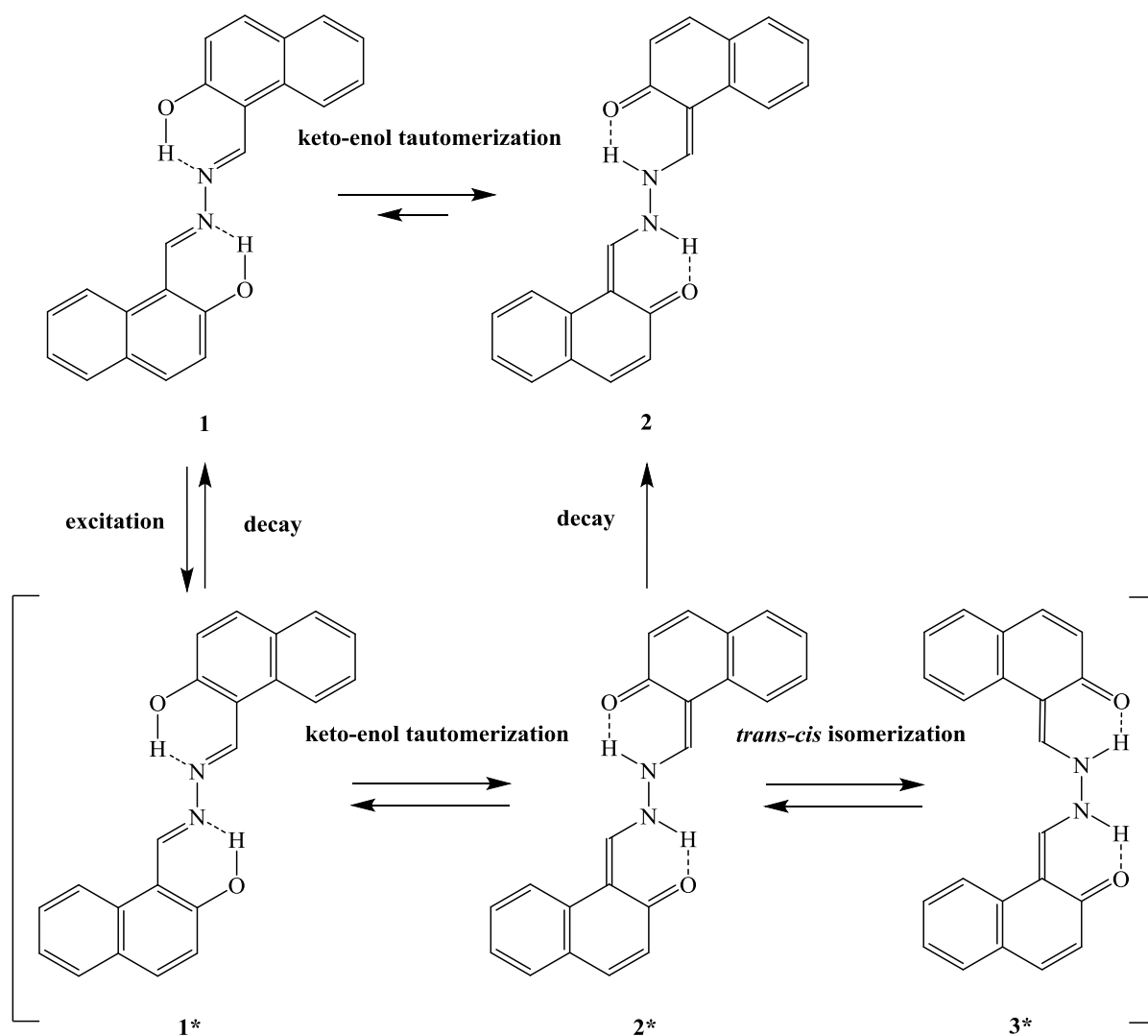
Scheme 1. Fluorescence, ESIPT, and isomerization of P.Y.101 ground and excited states.

TD-DFT predicts that excitation into the S_1 state leads to equilibration of the bonds in the azomethine portion (C-C, CN, and N-N),[2] while a CNN bending motion of this moiety has been identified to be the reaction coordinate along which efficient fluorescent quenching takes place in both the solid and solution.[5] Single crystal X-ray studies of substituted and free phenolic derivatives showed that intermolecular distances within the lattice are significantly lower than the 5-6 Å which would normally promote electron-transfer (ET) quenching. Although lower intermolecular distances generally facilitate non-radiative decay (such as electron transfer or charge transfer), PY101 uniquely retains excited state energy level characteristics within the crystal structure as the required charge-transfer states are inaccessible.

The aggregation-induced emission enhancement (AIEE) characteristics of P.Y.101 has recently been studied, in DMF/H_2O solution, by spectroscopic techniques, SEM, fluorescence microscopy, and X-ray crystal structure analysis.[7] This analysis indicates that rotation about the N-N bond is hindered by intramolecular hydrogen-bond formation, as well as the ordered intermolecular stacking and increase in the effective conjugation length resulting from aggregate formation, thus inhibiting non-radiative transitions and increasing the fluorescence quantum yield. In certain cases, an increase in fluorescence emission was also explained by the blocking of photo-induced electron transfer (PET) from the azine nitrogens to the other parts of the conjugated system, when these nitrogens, as well as the phenolic OH groups, participate in other interactions (*e.g.* complexation). This tunable off-on fluorescent behaviour gives P.Y.101 great potential in the selective detection of cations, *e.g.* Zn^{2+}.

In this work, we report the electron density obtained from high-resolution X-ray diffraction on the crystalline form of P.Y.101. Unlike the previous studies discussed above that deal largely with isolated gas-phase molecules, this approach includes crystal field effects as a matter of course. Of particular interest is the balance between intra- and inter-molecular hydrogen bonds, as well as the bonding with in the central chromophore. These experiments are supplemented with DFT calculated data on single molecules and dimers of P.Y.101.

Experimental

Crystal Preparation. The crystal used in this study was synthesised according to the method of Mathur *et al.*[3] All reagents were purchased from Sigma-Aldrich and used without further purification. P.Y.101 was dissolved in acetone and recrystallized by slow evaporation. A single crystal of **1**, in the form of a yellow block was obtained, with dimensions of 0.25 x 0.25 x 0.20 mm.

X-ray Data Collection and Reduction. The single crystal X-ray diffraction experiments were carried out at The University of Sydney using an Agilent Technologies SuperNova CCD-based diffractometer with an X-ray wavelength of 0.71043Å (MoKα).

The single crystal X-ray diffraction experiments were carried out at the University of Sydney using an Agilent Technologies SpuerNova CCD-based diffractometer with an X-ray wavelength of 0.7107 Å (Mo *Kα*) and at an experimental temperature of 100 K. A yellow single crystal of **1** was mounted onto the tip of a thin glass fibre with the minimum amount of

Paratone N oil, which acts as a cryoprotectant and adhesive, and inserted in the cold N_2 stream from an Oxford Cryosystems Cobra cooler. X-ray diffraction data were collected using 1.0° ω-scans maintaining the crystal-to-detector distance at 5.3cm. Reciprocal space was covered by positioning the detector arm at two different setting angles in 2θ, -41.5 and -90.5°, with corresponding exposure times of 20 and 65 s/frame. A total of 4652 frames were collected for the low- and medium-angle data, while 2948 frames were measured at the high angle. The data integration and reduction were undertaken with CrysAlis[Pro],[8] and the unit cell parameters for **1** at 100 K were refined from 10000 reflections in the monoclinic space group $P2_1/n$ with $Z = 2$, $F(000) = 356$, and $\mu = 0.090$ mm^{-1} (Table 1).

Refinement Strategies

The structure of **1** was solved using direct methods (SHELXS-97)[9] and full-matrix least-squares refinement on F^2 was carried out using SHELXL-97. All non-hydrogen atoms were refined anisotropically. Bond lengths to hydrogen atoms were fixed at neutron positions as obtained from average neutron diffraction values available in Brown *et al.*.[10] The coordinates and temperature factors obtained from the Independent Atom Model (IAM) refinement were imported into the multipole refinement program XD,[11] which uses a least-squares procedure to refine a rigid pseudoatom model in the form of the Hansen-Coppens multipole formalism.[12]

In a crystal the electron density $\rho(r)$ can be described by a sum of aspherical pseudoatoms with nuclear positions $\{R_j\}$:

$$\rho(r) = \sum_j j\rho_j(r - R_j)$$

With the pseudoatomic density form of:

$$\rho_j(r_j) = P_c\rho_c + \kappa'^3 P_v\rho_v(\kappa'r) + \kappa''^3 \sum_{l=0}^{l_{max}}\sum_{m=-l}^{m=1} P_{lm}R_l(\kappa''r_j)d_{lmp}(\theta_j,\phi_j)$$

The expression for the pseudoatom density includes the usual spherical core, a term to describe the spherical component of the valence density, plus a deformation term describing the asphericity of the valence density. The radial functions $\{R_l(r_j)\}$ are modulated by angular functions $\{d_{lmp}(\theta_j,\phi_j)\}$, defined by axes centred on each atom. A number of radial functions may be used, the most common being Slater-type functions.[13]

The starting point for the multipole refinement is the result of high-order spherical atom refinement ($\sin\theta/\lambda > 0.7$). The lengths of the bonds to hydrogen atoms in the O–H and C–H bonds were constrained to average neutron data values of 0.967 and 1.087 Å, respectively, with the heavy atom – hydrogen vectors taken from the spherical refinement; the multipole refinement was carried out using the least-squares part of the XD program package, and only reflections with $I > 2\sigma$ (I) were included in the refinement. The scale factor and temperature factors were refined separately. Subsequently, the multipoles were stepwise included in the refinements, ultimately reaching octapole level for O, N and C ($l_{max} = 3$).

The expansion was truncated at the octapole level with each heavy-atom assigned a κ', with a single κ' refined for each atom type. Hydrogen atoms were treated with one monopole and a fixed κ' of 1.2, with the aspherical density modeled by a single bond directed dipole ($l_{max} = 1$). Atomic positions and temperature factors were fixed at the values obtained from the high-order refinement described above. The refinements were continued until convergence and the Hirshfeld rigid bond test[14] was applied on the final models with an average value of the difference of mean-square thermal displacement amplitudes of 4×10^{-4} Å^2. This refinement is designated as exp in this manuscript.

Hydrogen Atom Treatment.

Following the detailed discussion by Wozniak,[15] anisotropic temperature factors for hydrogen atoms were calculated.[16] The parent heavy atom−hydrogen bond vector and distance were kept fixed as in the original multipole refinement, and additional refinements were carried out where the level of multipole expansion of the hydrogen atoms was increased to the full dipolar level (this refinement is designated *Shade* in this manuscript).

Further crystallographic details are given in Table 1 and in the Supporting Information. The complex **1** is shown in Figure 1a (isotropic hydrogen atoms) and 1b (anisotropic displacements for hydrogen estimated by SHADE2[17], both with thermal ellipsoids at the 50% probability value.
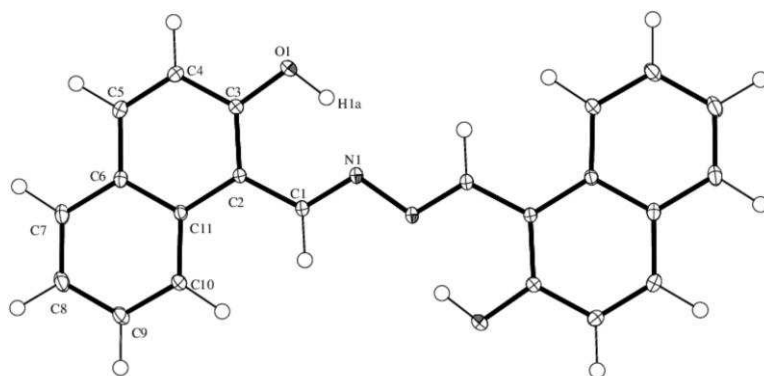
(a)
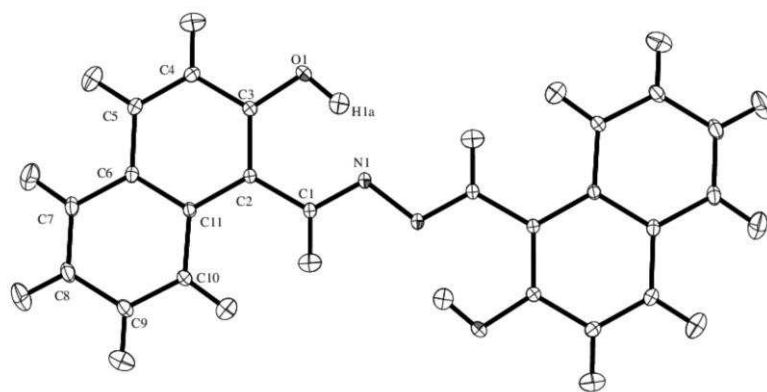
(b)

Figure 1 Molecular structure of 1, (a) isotropic hydrogen atoms, and (b) *Shade* estimated anisotropic displacements for hydrogen atoms.

Theoretical calculations. Density functional theory (DFT) data were calculated using the hybrid B3LYP functional[17] with a 6-31+G** basis set[18] in the Gaussian09 suite.[19] Tests on a single molecule show that calculated density properties vary little with different choice of functional and/or larger basis sets (Table S4). For intramolecular studies, a single molecule of **1** was isolated from the final multipole-refined structure, and geometry optimised in gas phase. This resulted in a planar structure with no imaginary frequencies, confirming this as a true minimum and indicating that the slight non-planarity in the crystal stems from packing forces. For intermolecular studies, a dimer of symmetry-related molecules was extracted and

X-ray coordinates used without further modification. All analysis of theoretical densities used the AIMAll package.[20]

Table 1 Crystallographic details for **1**.

|	**1**
Formula	$C_{22}H_{16}N_2O_2$
Molecular Mass	340.37
Crystal size (mm^3)	0.25 x 0.25 x 0.20
Temperature (K)	100 (2) K
Crystal system	Monoclinic
Space group	$P2_1/n$
a (Å)	8.369 (3)
b (Å)	6.014 (4)
c (Å)	15.892 (5)
α (º)	90.00
β (º)	91.670 (1)
γ (º)	90.00
Volume ($Å^3$)	816.061 (5)
Z	2
Refinement Method	Full-matrix least squares
No. of reflections collected	141575
No. unique data	13516
R_{int}	0.038
No. reflections used (I > 2σI)	11130
Data:Parameter ratio	90.1
ρ_c (gcm^{-1})	1.385
F(000)	356.0
μ (mm^{-1})	0.090
sin θ/λ_{max}	1.28 $Å^{-1}$
θ range for data collection (°)	4.13 – 65.43
Index ranges	-21 =< h =< 21, 0 =< k =< 15, 0 =< l =< 40

Residual density ($e\text{Å}^{-3}$)	0.610, -0.320 eÅ^{-3}
Final R1, wR2	0.0372, 0.1058
Goodness of fit	1.026
Completeness	97.7%
Multipole Refinement	
No. of reflections I>2σ(I) (N_{ref})	11130
Refined on	F_o^2
N_{ref}/N_{var} (exp / Shade)	49.4 / 36.37
$R_w(F), R_w(F^2) > 2\sigma(F)$	0.024, 0.044
$R(F), R(F^2),$ all data	0.030, 0.056
(Shade) $R_w(F), R_w(F^2) > 2\sigma(F)$	0.030, 0.046
(Shade) $R(F), R(F^2),$ all data	0.027, 0.055
Goodness of fit	1.34
(Shade) Goodness of fit	1.33

Figure 2 illustrates the residual density obtained from the final refinement, demonstrating a virtually featureless landscape (*max.* 0.16e.Å^{-3}) across the entire molecule and hence successful application of the multipole model. Figure 3 contains the static deformation density from the same model, and displays significant maxima in all covalent bonds, as well as the expected lone pair regions of N(1) and O(1). There are no double maxima observed in the deformation density, again adding weight to the quality of the data / refinement. However, it is apparent that the concentration of density in the N(1)—N(1)′ bond is markedly less than that observed in C-N and C-C bonds. This point will be discussed in more detail below.
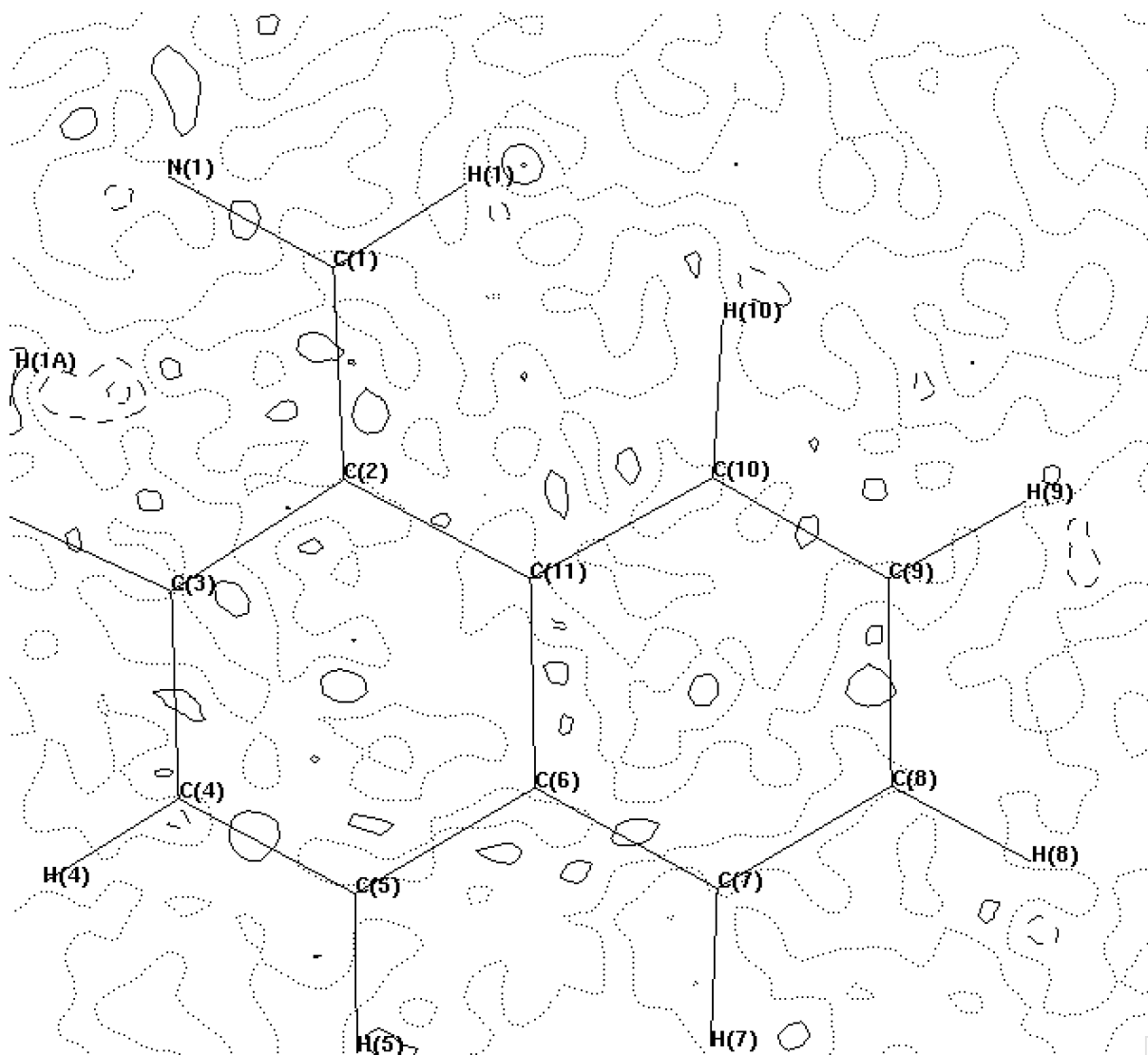
**Figure 2** Residual density from multipole model in the plane of C(1), N(1) and C(2), displayed at the 0.1 e.Å^{-3} contour level.
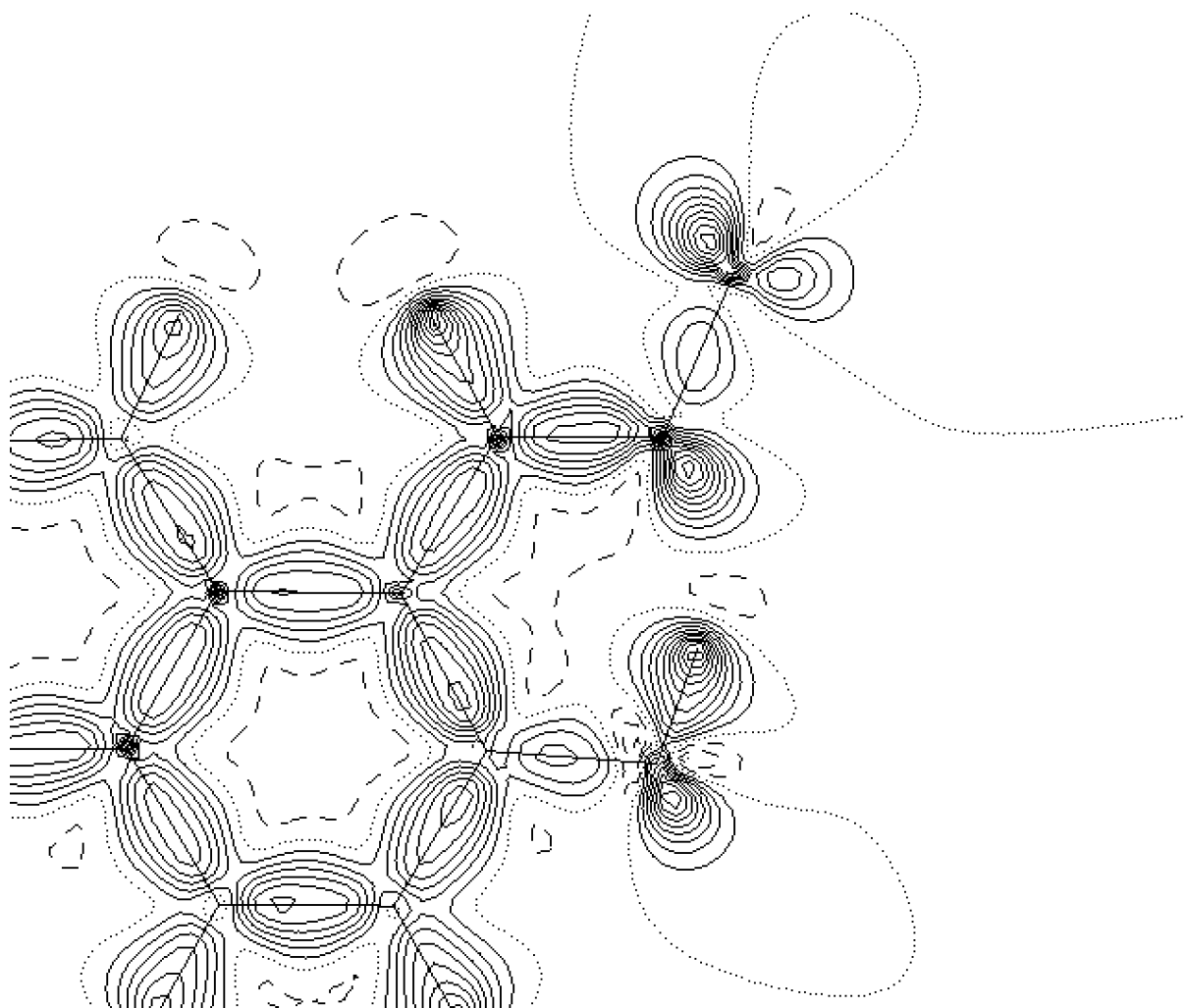
Figure 3: Static deformation density in plane of C(1), N(1) and C(2), plotted with contours at regular the 0.1 e.Å^{-3} intervals.

Table 2 Topological analysis of selected intramolecular covalent bonds. Values in the first row are obtained from multipole refinement, in the second row from the SHADE refinement and the third row from B3LYP/6-31+G**.

| Bond	ρ / eÅ^{-3}	$\nabla^2\rho$ / eÅ^{-5}	ε	R_{ij} / Å	d_1 / Å	d_2 / Å
N(1)-N(1)	2.21	-2.54	0.06	1.385	0.694	0.691
Shade	2.24	-2.46	0.05	1.387	0.695	0.691
DFT	2.34	-16.03	0.04		0.689	0.689
O(1)-C(3)	2.14	-19.16	0.11	1.341	0.811	0.530
	2.16	-18.90	0.09	1.343	0.811	0.531
	2.06	-8.68	0.00		0.896	0.446
O(1)-H(1A)	2.59	-26.23	0.02	0.967	0.716	0.251
	2.15	-27.64	0.02	0.967	0.757	0.210
	2.20	-44.23	0.02		0.812	0.186
N(1)-C(1)	2.53	-26.68	0.24	1.299	0.773	0.526
	2.55	-26.95	0.24	1.300	0.776	0.524
	2.48	-19.51	0.18		0.861	0.443
C(1)-C(2)	1.92	-14.27	0.21	1.446	0.734	0.712
	1.91	-14.47	0.20	1.446	0.734	0.712
	1.94	-17.94	0.16		0.742	0.702

Table 2 reports topological properties of selected intramolecular covalent bonds. These data support the suggestion by Dreuw *et al.* that assignment of the ground state of **1** contains localised C=N—N=C bonding, as evidenced by from the larger density and more negative Laplacian, as well as raised ellipticity, in N(1)-C(1) compared to N(1)-N(1)′ or C(1)-C(2). Values for C-C bonds in the naphthyl moiety are in expected ranges for aromatic bonds, and so are not reported in the main text (complete data can be found in Supporting Information, Table S2). We also see evidence for the relative strength of C-O and O-H bonds, which both display properties comparable with C-C bonds. In general the agreement between experiment and theory is excellent, but the Laplacian value in the central N-N bond has quite different values between experiment and theory, the latter indicating a markedly stronger bond that experiment. This is despite the fact that the electron density at the N—N bcp is almost identical between methods. This is discussed in more detail below.
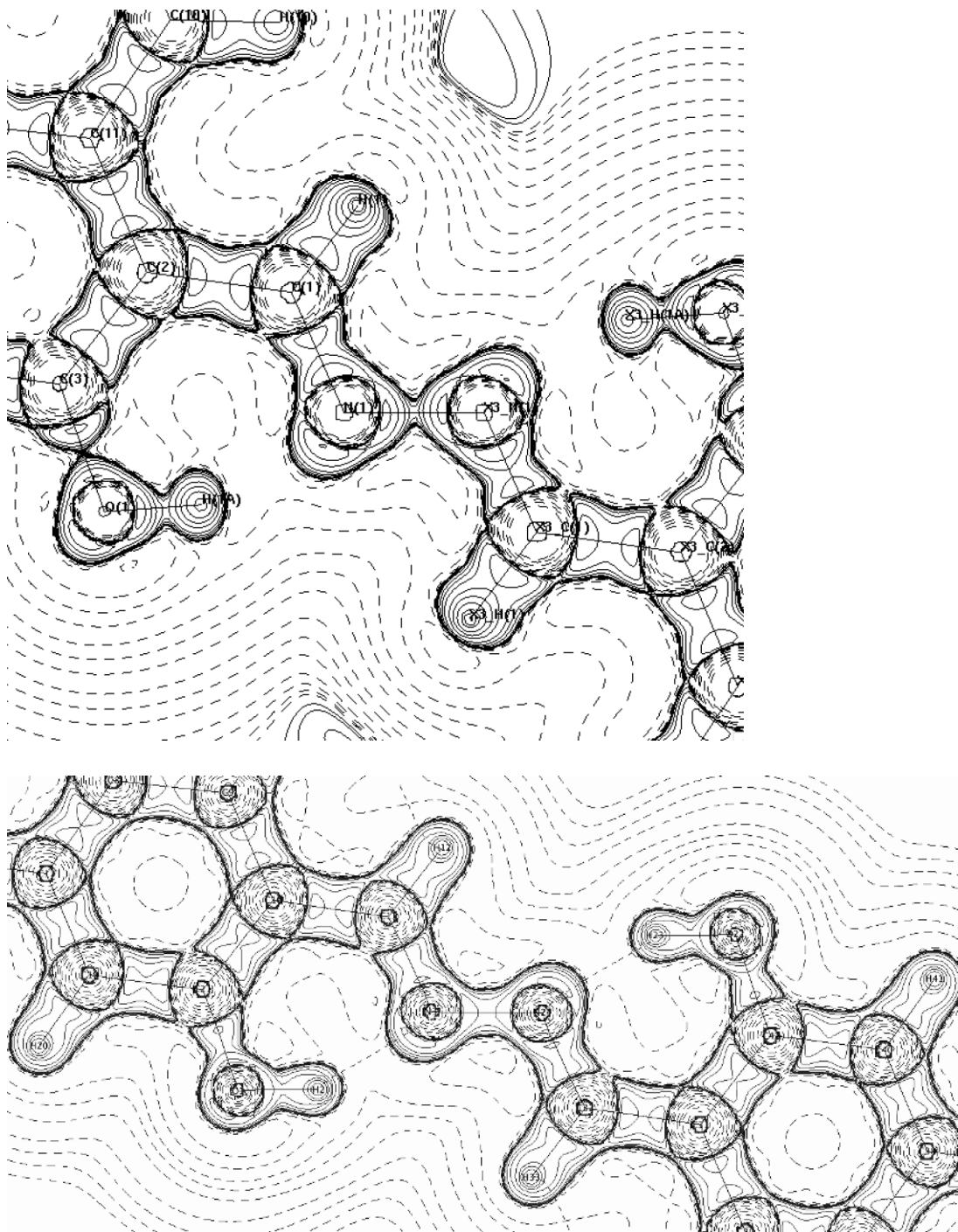
Figure 4 Laplacian plots from a) experiment, and b) theory.

Figure 4 shows contour plots of the Laplacian of the electron density in the central portion of the molecule, from both experiment and DFT. Agreement between methods in most bonds and expected lone pair regions is generally excellent. However, the behaviour of the N—N bond differs significantly: the experimental map exhibits noticeable "pinching" of the valence shell charge concentration (VSCC) in this bond, whereas theory shows no evidence of this.

This effect has been seen before in polar bonds[21,22], but the non-polar nature of this bond appears to rule this out as an explanation. To further check the agreement between experiment and theory, we also plotted the total electron density in the same plane (Figure S1): as with topological data, this shows excellent agreement between experiment and theory. Figure 5 shows the total density and Laplacian plotted along the N—N bond. The density exhibits a slight discrepancy (up to 0.3 e.Å^{-3}) between 0.2 and 0.5 Å from each nucleus. In the region of the bcp, agreement seems excellent on the scale shown in Figure 5, but as reported in Table 2 the experimental density is lower by *ca*. 0.1 e.Å^{-3} at the bcp itself. The effect of this subtle change is more obvious in the equivalent Laplacian plot The combination of lower density at the bcp and higher density between 0.2 and 0.5 Å from each nucleus obtained by the multipole model means that the curvature of the density parallel to the bond *must* be greater in the experimental results than in theoretical results in a more pronounced minimum compared to DFT data. This effect is seen more clearly in a plot of density close to the bcp (Figure S2), where the experimental data clearly changes more quickly than the theoretical counterpart. Thus, very small differences in the total electron density, of the same magnitude as the residual errors stemming from the multipole model, are amplified in the Laplacian into apparently major discrepancies between experiment and theory.
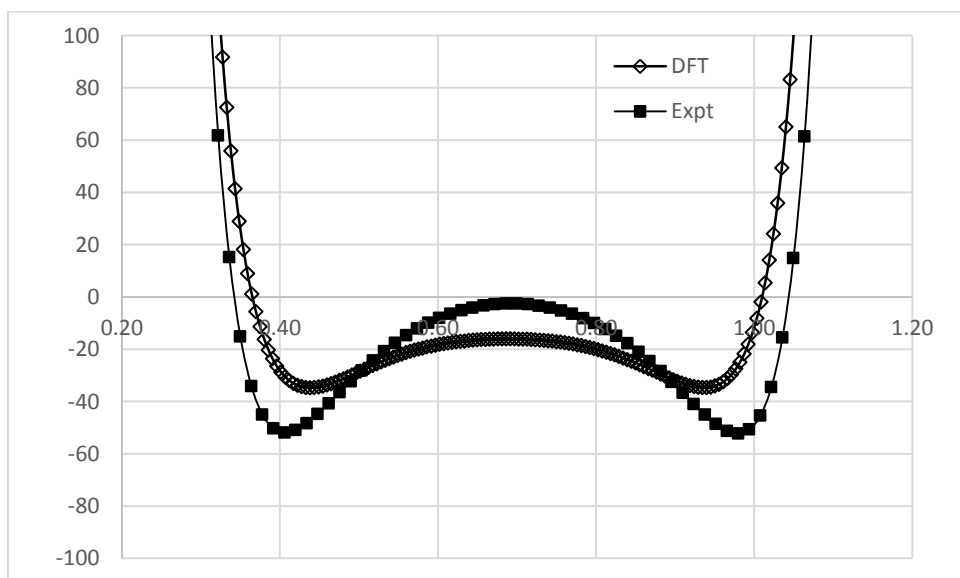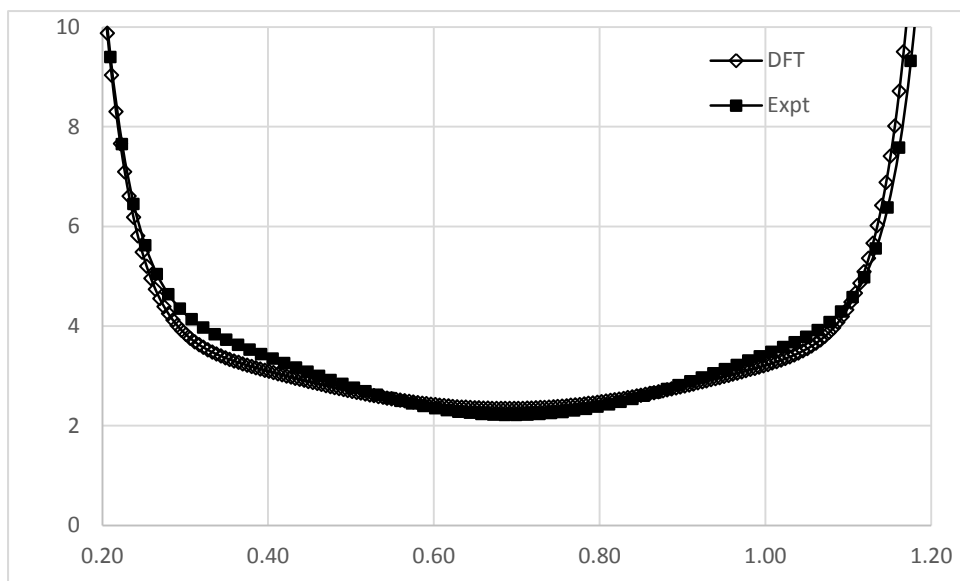
Figure 5 Electron density (top) and Laplacian (bottim) plots along N—N bond from experiment and theory.

Figure 4 also highlights the presence of a large area of charge concentration in the expected lone pair region on N(1), the properties of which will be important for the intramolecular hydrogen bond formed with H(1a). Searching the Laplacian of the density finds the critical point in this function associated with this. Experimental values at this point are $\rho = 3.95(1)$ eÅ^{-3}, $\nabla^2\rho = -84.98(1)$ eÅ^{-5}, r = 0.391 Å. DFT properties are $\rho = 3.93$ eÅ^{-3}, $\nabla^2\rho = -75.47$ eÅ^{-5}, r = 0.389 Å. This lone pair forms a C(1)-N(1)-LP angle of 125.6(2) (experimental) /121.3

(theory), thus placing it in the position expected of the sp^2-hybridised N(1). This also means that the intramolecular H-bond is not linear, instead forming a N(1)-LP-H(1A) angle of 146.2(1) / 143.6 (theory) degrees. This is in reasonable agreement with the N(1) H(1A) – O(1) angle of 150.9 but is, surprisingly, indicative of the lack of polarisation of the LP toward the hydrogen atom given the strength of the bond (*vide infra*).

Table 3 Topological analysis of hydrogen bonding. Values in the first row are obtained from multipole refinement, *Shade* refers to values from refinement to anisotropic Hydrogen atoms at the dipolar (l_{max}=1) level of multipole expansion, and in the third row from B3LYP/6-31+G** gas phase calculation. Standard uncertainties have been omitted from the table for clarity. They are closely scattered around 0.02 e $Å^{-3}$ (ρ_{bcp}) and 0.05 e $Å^{-5}$ ($\nabla^2\rho_{bcp}$).

	ρ /e$Å^{-3}$	$\nabla^2\rho$ /e$Å^{-5}$	ε	G /E_h e$Å^{-3}$	V /E_h e$Å^{-3}$	H /E_h e$Å^{-3}$	E_{HB} /kJ mol^{-1}
Intramolecular							
N(1)···H(1A)–O(1)	0.33	5.53	0.07	0.39	-0.39	0.00	151.7
Shade	0.32	4.34	0.06	0.33	-0.35	-0.02	136.2
DFT	0.36	2.92	0.04	0.24	-0.28	-0.04	108.0
H(10)···H(1)	0.09	1.25	5.17	0.07	-0.06	0.01	23.4
	-	-	-	-	-	-	-
	0.09	1.24	0.45	0.07	-0.05	0.02	20.0
Intermolecular							
C(9)···H(1)–C(1)	0.02	0.19	0.29	0.01	-0.01	0.00	3.9
	0.01	0.28	0.00	0.01	-0.01	0.01	3.9
	0.06	0.62	0.45	0.04	-0.03	0.01	10.4
C(8) ··· H(1) – C(1)	0.03	0.43	0.52	0.02	-0.02	0.01	7.8
	0.03	0.44	0.49	0.02	-0.01	0.01	3.9
	0.05	0.62	0.44	0.03	-0.03	0.01	11.7
C(2)…H(9)-C(9)	0.01	0.21	0.00	0.01	-0.01	0.00	3.9
	0.02	0.28	0.57	0.01	-0.01	0.01	3.9
	0.02	0.24	3.15	0.01	-0.01	0.00	3.7
O(1)···H(9)–C(9)	0.04	0.79	0.40	0.04	-0.03	0.01	11.6

	0.04	0.75	0.32	0.04	-0.03	0.01	11.6
	0.05	0.75	0.02	0.05	-0.04	0.01	14.9
O(1)…H(8)-C(8)	0.02	0.33	0.28	0.02	-0.01	0.01	3.9
	0.02	0.30	0.47	0.01	-0.01	0.01	3.9
	0.02	0.34	14.2	0.02	-0.01	0.01	4.5
N(1)…H(8)-C(8)	0.02	0.29	1.10	0.01	-0.01	0.01	3.9
	0.02	0.28	0.57	0.01	-0.01	0.01	3.9
	0.03	0.33	0.32	0.02	-0.01	0.00	5.3
C(10)…H(10)-C(10)	0.01	0.22	0.49	0.01	-0.01	0.00	3.9
	0.01	0.24	0.36	0.01	-0.01	0.01	3.9
	0.03	0.33	0.32	0.02	-0.01	0.00	5.3

As suggested by Abramov[23], the kinetic and potential energy densities (G and V) and the total energy density (H) at bond critical points in hydrogen bonds can be determined from the density property V, and thus can be used as a measure of bond strength. The ratio –G/V can also be used to estimate covalency in H-bonds: a value of between 0.5 and 1 indicates partly covalent character, while a value of greater than 1 is purely non-covalent.[24] Data from Table 3 suggest some covalent character in N(1)···H(1A)–O(1), with values between 0.86 and 1.0 depending on method. All other interactions in Table 3 exhibit values of 1.0 or greater.

Additionally the method established by Espinosa[25] allows the estimation of the interaction energies, using the following correlation:

$$E_{HB} = \tfrac{1}{2}\{\{\tfrac{1}{4}\nabla^2\rho(r_{cp})\} - \{\tfrac{3}{4}(3\pi^2)^{2/3}(\rho(r_{cp})^{5/3} + \tfrac{1}{6}\nabla^2\rho(r_{cp})\}\}$$

Table 3 reports analogous data for intra- and inter-molecular non-covalent interactions in **1**. Again, agreement between experimental and DFT data is generally excellent, as indeed it is for geometrical details of intramolecular contacts (Table S3). By any measure used, the intramolecular N—H…O hydrogen bond is the most significant of these; the density at the associated bcp is very large for a neutral H-bond,[26] as is the potential energy density. However, the latter is balanced by large positive kinetic energy here, such that the overall energy density is close to zero. H-bond strengths predicted from these energy densities using Abramov's method are very large indeed; the value of over 150 kJ mol^{-1} exceeds the accepted

ranges for neutral H-bonds and indeed many charged interactions.[27] We examine this issue in more detail below. Within a single molecule of **1** we also find a bcp and bond path between hydrogens: such interactions have been widely reported in planar aromatic species, and the properties reported in Table 3 are in typical ranges of these.[28]

The need for calculated anisotropic displacement parameters for hydrogen atoms

In modern charge density studies, it has become increasingly popular to calculate theoretical anisotropic displacement parameters for hydrogen atoms[15,16] in the absence of neutron diffraction data. This is done in an attempt, for example, to provide a more robust description of the electron distribution in Hydrogen bonding interactions. A recent publication[29] reported that this approach should be used judiciously, and it was stressed that this should not be applied as a general method, but rather adopted on a case-by-case basis, as it can lead to spurious values of the density and thus inaccurate descriptions of H-bond strengths.

As standard in charge density studies, it is customary to check the results of the multipole refinement against high-level theoretical calculations in order to compare the intramolecular topology of the density. Table S6 (Supplementary data) outlines the differences in ρ, $\nabla^2\rho$ in the heavy atom – hydrogen bcps. The maximum deviation between the experimental value of ρ and $\nabla^2\rho$ and those from the Shade model is 0.41, *ave.* 0.25 eÅ^{-3}, and in $\nabla^2\rho$ the maximum difference is 1.41, *ave.* 0.43 eÅ^{-5}. The two models are almost the same, with both consistently underestimating the values of both the density and Laplacian at the bcps compared to DFT; although the experimental value could be considered slightly more in line with the theoretical topology, this is marginal.

In the work of Nguyen *et al*[29], it was found that the application of the Shade model displayed the most significant differences in the intermolecular interactions, but in this case we see that both *Exp* and *Shade* refinements are in close agreement for intramolecular bonds to H, with both consistently underestimating the density when compared to that of the DFT calculation.

It is interesting to note that the *exp* and *Shade* refinements are essentially the same regarding hydrogen bonding properties (Table 3), with one notable exception: it proved impossible to locate the H(10)…H(1) intramolecular bond, and when relaxing the bcp search parameters often returned a physically unreasonable negative density, at bond bcps. This points to the

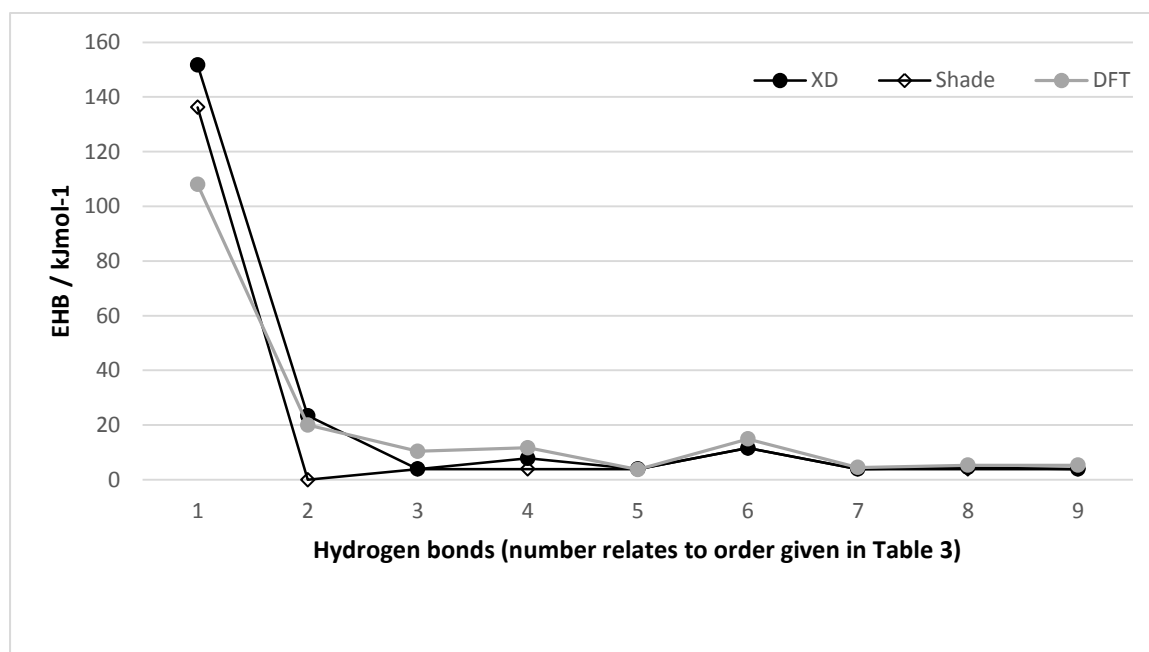Shade refinement introducing systematic errors, perhaps due to over-parameterisation of the multipole model.

Figure 6 Graph of difference in H-bond energies for *Exp, Shade* and DFT.

Figure 6 displays the differences in the hydrogen bond energies, and it can be clearly seen that the *Exp* refinement returns values closer to the DFT result, with the one exception of the N(1)…H(1A) bond. We discuss the strength of this interaction in more detail below. Clearly, the use of anisotropic hydrogen atoms in the *Shade* refinement has very little to recommend it in this system, and introduces some uncertainties in the topological analysis. Further work is certainly required to substantiate the use of the method as standard in experimental charge density studies.

As well as intramolecular contacts, the crystal structure of **1** contains numerous intermolecular interactions. In total, we find bcps associated with 2 C—H…O, 1 C—H…N and 3 C—H…π hydrogen bonds. Based on the density properties in Table 3, these intermolecular H-bonds are substantially weaker than the intramolecular N—H…O interaction. This is vital for the observed solid-state fluorescence of **1**, since the relative strength of intra- over inter-molecular interactions means that the properties of an isolated

molecule carry over into the solid state. Moreover, it seems that the intramolecular N—H…O H-bond effectively "sequesters" the OH within a single molecule, thereby providing a rationale for this species contradicting an empirical rule that states that pigments with OH groups usually do not fluoresce.[2]

The very large estimates of strength for the intramolecular N—H…O H-bond based on experimental and theoretical energy densities prompted us to carry out further theoretical tests of this important aspect of the chemistry and photophysics of **1**. Estimation of intramolecular H-bond strength is not straightforward due to difficulty in defining a reference state, so we have taken several approaches to this. Firstly, rotation about C(1)-C(2) by 180° yields an *endo*-diol species that contains only one such H-bond rather than two in the optimal *trans*-diol geometry, and is 46.1 kJ mol^{-1} higher in energy than the global minimum. However, this *endo*-diol contains a close OH…HC contact (1.727 Å) that may destabilise this reference state and so lead to overestimation of H-bond strength. The transition state for conversion between *trans* and *endo* diols, which contains no such contact, lies 55.3 kJ mol^{-1} above the global minimum, but may be destabilized by loss of conjugation as well as of H-bonding. An alternative reference state, formed by rotating the OH group out of the molecular plane by 90° rotation about C(3)-O(1), increases DFT energy by 84.7 kJ mol^{-1}. Once again, this reference state may be destabilized by effects other than loss of H-bonding, *i.e.* repulsion between O(1) and N*(1). Finally, 2,4'-dihydroxy-1,1'-naphthalazine formed by placing the OH group *para* to the azomethine moiety is 33.3 kJ mol^{-1} above the *ortho* form in **1**. While these estimates differ significantly, none approach the 150 kJ mol^{-1} value obtained from topological analysis. Moreover, since we suspect that the first three are overestimates, we would tentatively assign the strength of the N—H…O H-bond in **1** to be in the region of 30 to 40 kJ mol^{-1}. This analysis therefore casts doubt on the suitability of Espinosa's approach to estimation of H-bond strength in cases such as this. Previous work has shown that consideration of bcp properties alone is insufficient to characterize all aspects of hydrogen bonding, for instance suggesting the Interacting Quantum Atoms (IQA) approach instead.[30] However, such properties cannot be extracted from experimental data at present.

Conclusions

In this study, we have determined the high-resolution electron density distribution of an organic pigment, P.Y.101 (**1**) that, unusually, retains its fluorescence in the solid state. The

density that stems from using the multipole formalism on high-resolution X-ray diffraction data is compared with that from theoretical calculations. Excellent agreement between experiment and theory is found in general, but in the case of the Laplacian of the density in the central N(1)—N(1)′ bond we observe significant difference. Closer inspection of the density and Laplacian in this bond reveals small deviations (0.1 to 0.3 eÅ^{-3}) in total density between methods. Crucially, these differences differ in sign between the bond midpoint and regions 0.2 to 0.5 Å from nuclei, leading to significantly greater curvature of the density parallel to the bond direction. Since the Laplacian is simply the sum of these curvatures, the small differences in density are amplified into substantial changes in Laplacian.

We have paid particular attention to the hydrogen bonds both within and between molecules of **1**, due to their crucial importance in determining the photophysics of **1** in the solid state. Both experiment and theory highlight the remarkable strength of the intramolecular N—H…O H-bond, which exhibits density properties right at the limit of those previously observed for neutral H-bonds. We also find evidence for non-covalent H…H interactions in the extended π-system of **1**, as previously observed in polycyclic aromatics. Intermolecular H-bonds of type C—H…O, C—H…N and C—H…π are located by both experiment and theory, for which agreement is again excellent. As judged by the density and Laplacian values at the H-bond critical point, these intermolecular contacts are much weaker than the intra-molecular N—H…O one. However, when applying the method for estimation of hydrogen bond energies derived from energy densities, we arrive at a suspiciously large value of over 150 kJ mol^{-1}. DFT estimates based on reference states that have been rotated or chemically altered to remove the N—H…O H-bond lie between 30-80 kJ mol^{-1}, squarely in the range expected for neutral H-bonds. It therefore appears that such close intramolecular contacts are not suitable for the application of this approach.

The use of theoretically derived anisotropic displacement parameters on hydrogen atoms has been shown to have very little impact on the density properties for this system, especially when describing the topology of hydrogen bonding This leads us to question the validity of the perceived need to use this method in charge density studies. We stress that this should be judged on a case-by-case basis, and not applied as a 'fits all' approach.

Electronic Supplementary Information (ESI) available:

Geometrical data including bond lengths and angles plus intra- and inter-molecular hydrogen bonds; topological data for all covalent bonds; total electron density contour plots; plots of total electron density ±0.1 Å from N—N bcp.

References

[1] W. Herbst and K. Hunger, *Industrial Organic Pigments: Production, Properties, Applications*, Wiley, 2006

[2] A. Dreuw, A. Plotner, L. Lorenz, J. Wachtveitl, J. E. Djanhan, B. Bruning, T. Metz, M. Bolte and M. U. Schmidt, *Angew. Chem.-Int. Edit.*, 2005, **44**, 7783.

[3] S. S. Mathur and H. Suschitzky, *J. Chem. Soc.-Perkin Trans. 1*, 1975, 2479.

[4] J. Plotner and A. Dreuw, *Phys. Chem. Chem. Phys.*, 2006, **8**, 1197.

[5] J. Plotner and A. Dreuw, *Chem. Phys.*, 2008, **347**, 472.

[6] L. Lorenz, J. Plotner, V. V. Matylitsky, A. Dreuw and J. Wachtveitl, *J. Phys. Chem. A*, 2007, **111**, 10891.

[7] X. Cao, X. Zeng, L. Mu, Y. Chen, R.-x. Wang, Y.-q. Zhang, J.-x. Zhang and G. Wei, *Sensors and Actuators B: Chemical*, 2013, **177**, 493.

[8] Agilent, (2012), *CrysAlis PRO*. Agilent Technologies UK Ltd, Yarnton, England..

[9] , G. M. Sheldrick (2008). *Acta Cryst.* A**64**, 112-122.

[10] G. M. Brown and H. A. Levy, *Acta Cryst. B*, 1973, **29**, 790.

[11] T. H. Koritsanszky, S. T.; Richter, T; Mallinson, P. R.; Su, Z.; Hansen, N. K., *XD. A Computer Program Package for Multipole Refinement and Analysis of Charge Densities from X-ray Diffraction Data;*, (1998) Free University of Berlin:, Berlin, Germany.

[12] N. K. Hansen and P. Coppens, *Acta Cryst. A*, 1978, **34**, 909.

[13] W. J. Hehre, R. F. Stewart and J. A. Pople, *J. Chem. Phys.*, 1969, **51**, 2657.

[14] F. Hirshfeld, *Acta Cryst. A*, 1976, **32**, 239.

[15] A. A. Hoser, P. M. Dominiak, K. Wozniak, *Acta Crystallogr., Sect. A*, 2009, A65, 300.

[16] A. Ø. Madsen, J. Appl. Crystallogr. 2006, 39, 757.

[17] (a) A. D. Becke, *J. Chem. Phys.*, 1993, 98, 5648; (b) C. T. Lee, W. T. Yang and R. G. Parr, *Phys. Rev. B: Condens. Matter Mater. Phys.*, 1988, 37, 785.

[18] a) W. J. Hehre, R. Ditchfield and J. A. Pople, *J. Chem. Phys.*, 1972, **56**, 2257-2261. b) M. M. Francl, W. J. Pietro, W. J. Hehre, J. S. Binkley, M. S. Gordon, D. J. Defrees and J. A. Pople, *J. Chem. Phys.*, 1982, **77**, 3654-3665. c) T. Clark, J. Chandrasekhar, G. W. Spitznagel and P. V. Schleyer, *J. Comput. Chem.*, 1983, **4**, 294-301.

[19] M. J. Frisch, G. W. Trucks, H. B. Schlegel, G. E. Scuseria, M. A. Robb, J. R. Cheeseman, G. Scalmani, V. Barone, B. Mennucci, G. A. Petersson, H. Nakatsuji, M. Caricato, X. Li, H. P. Hratchian, A. F. Izmaylov, J. Bloino, G. Zheng, J. L. Sonnenberg, M. Hada, M. Ehara, K. Toyota, R. Fukuda, J. Hasegawa, M. Ishida, T. Nakajima, Y. Honda, O. Kitao, H. Nakai, T. Vreven, J. A. Montgomery Jr., J. E. Peralta, F. Ogliaro, M. Bearpark, J. J. Heyd, E. Brothers, K. N. Kudin, V. N. Staroverov, R. Kobayashi, J. Normand, K. Raghavachari, A. Rendell, J. C. Burant, S. S. Iyengar, J. Tomasi, M. Cossi, N. Rega, N. J. Millam, M. Klene, J. E. Knox, J. B. Cross, V. Bakken, C. Adamo, J. Jaramillo, R. Gomperts, R. E. Stratmann, O. Yazyev, A. J. Austin, R. Cammi, C. Pomelli, J. W. Ochterski, R. L. Martin, K. Morokuma, V. G. Zakrzewski, G. A. Voth, P. Salvador, J. J. Dannenberg, S. Dapprich, A. D. Daniels, Ö. Farkas, J. B. Foresman, J. V. Ortiz, J. Cioslowski and D. J. Fox, Gaussian 09 (Revision D.01), Gaussian, Inc., Wallingford, CT, 2009.

[20] T. A. Keith, Aimall (version 13.11.04), TK Gristmill Software, Overland Park KS, USA, 2013.

[21] D. E. Hibbs, J. R. Hanrahan, M.B. Hursthouse, D. W. Knight, J. Overgaard, R. O. Piltz, M. P. Waller, *Org Biomol Chem,* 2003, 1, (6), 1034.

[22] D. E. Hibbs, C. J. Austin-Woods, J. A. Platts, J. Overgaard, P. Turner, *Chemistry – A European Journal*, 2003, 9(5), 1075.

[23] Y. A. Abramov, Acta Cryst., 1997, **A53**, 264.

[24] M. Ziółkowski, S. J. Grabowski, J. LeszczynskiJ. Phys. Chem. A 2006, 110, 6514.

[25] E. Espinosa, E. Molins, C. Lecomte, Chem. Phys. Lett. 1998, **285**, 170.

[26] U. Koch and P. Popelier, *J. Phys. Chem.*, 1995, **99**, 9747.

[27] a) T. Steiner, *Angew. Chem. Int. Ed.*, 2002, **41**, 48; b) G. A. Jeffrey, *An Introduction to Hydrogen Bonding*, OUP, 1997.

[28] C. F. Matta, J. Hernandez-Trujillo, T.-H. Tang, R. F. W. Bader, Chem. Eur. J. 2003, **9**, 1940.

[29] T. H. Nguyen, S. T. Howard, J. R. Hanrahan, Paul W. Groundwater, J. A. Platts and D. E. Hibbs, J. Phys. Chem A., 2012, 116 (23), 5618.

[30] a) V. Tognetti and L. Joubert Phys. Chem. Chem. Phys. 2014, 16, 14539. b) A. Martín Pendás, M. A. Blanco and E. Francisco, J. Chem. Phys. 2006, 125, 184112.